





Bolaamphiphile Analogues of 12-bis-THA Cl₂ Are Potent Antimicrobial Therapeutics with Distinct Mechanisms of Action against Bacterial, Mycobacterial, and Fungal Pathogens

 Simona Di Blasio,^a  Maria Clarke,^a Charlotte K. Hind,^b Masanori Asai,^{c,d} Louis Laurence,^e Angelica Benvenuti,^a Mahnoor Hassan,^a Dorothy Semenya,^a DeDe Kwun-Wai Man,^{a,f} Victoria Horrocks,^a Giorgia Manzo,^a Sarah Van Der Lith,^a Carolyn Lam,^a Eugenio Gentile,^a Callum Annette,^a  Janine Bosse,^c Yanwen Li,^c Barry Panaretou,^a  Paul R. Langford,^c Brian D. Robertson,^d Jenny K. W. Lam,^{f,g} J. Mark Sutton,^{a,b} Michael McArthur,^e  A. James Mason^a

^aInstitute of Pharmaceutical Science, School of Cancer & Pharmaceutical Sciences, King's College London, London, United Kingdom

^bTechnology Development Group, UK Health Security Agency, Research and Evaluation, Salisbury, United Kingdom

^cSection of Paediatric Infectious Disease, Department of Infectious Disease, Imperial College London, London, United Kingdom

^dMRC Centre for Molecular Bacteriology and Infection, Department of Infectious Disease, Imperial College London, London, United Kingdom

^eNorwich Medical School, University of East Anglia, Norwich, United Kingdom

^fDepartment of Pharmacology & Pharmacy, Li Ka Shing Faculty of Medicine, The University of Hong Kong, Pokfulam, Hong Kong

^gDepartment of Pharmaceutics, UCL School of Pharmacy, University College London, London, United Kingdom

ABSTRACT 12-Bis-THA Cl₂ [12,12'-(dodecane-1,12-diyl)-bis-(9-amino-1,2,3,4-tetrahydroacridinium) chloride] is a cationic bolalipid adapted from dequalinium chloride (DQC), a bactericidal anti-infective indicated for bacterial vaginosis (BV). Here, we used a structure-activity-relationship study to show that the factors that determine effective killing of bacterial, fungal, and mycobacterial pathogens differ, to generate new analogues with a broader spectrum of activity, and to identify synergistic relationships, most notably with aminoglycosides against *Acinetobacter baumannii* and *Pseudomonas aeruginosa*, where the bactericidal killing rate was substantially increased. Like DQC, 12-bis-THA Cl₂ and its analogues accumulate within bacteria and fungi. More hydrophobic analogues with larger headgroups show reduced potential for DNA binding but increased and broader spectrum antibacterial activity. In contrast, analogues with less bulky headgroups and stronger DNA binding affinity were more active against *Candida* spp. Shortening the interconnecting chain, from the most lipophilic twelve-carbon chain to six, improved the selectivity index against *Mycobacterium tuberculosis in vitro*, but only the longer chain analogue was therapeutic in a *Galleria mellonella* infection model, with the shorter chain analogue exacerbating the infection. *In vivo* therapy of *Escherichia coli* ATCC 25922 and epidemic methicillin-resistant *Staphylococcus aureus* 15 (EMRSA-15) infections in *Galleria mellonella* was also achieved with longer-chain analogues, as was therapy for an *A. baumannii* 17978 burn wound infection with a synergistic combination of bolaamphiphile and gentamicin. The present study shows how this class of bolalipids may be adapted further to enable a wider range of potential applications.

IMPORTANCE While we face an acute threat from antibiotic resistant bacteria and a lack of new classes of antibiotic, there are many effective antimicrobials which have limited application due to concerns regarding their toxicity and which could be more useful if such risks are reduced or eliminated. We modified a bolalipid antiseptic used in throat lozenges to see if it could be made more effective against some of the highest-priority bacteria and less toxic. We found that structural modifications that rendered the lipid more toxic against human cells made it less toxic in infection models and we could effectively treat caterpillars infected with either *Mycobacterium tuberculosis*, methicillin resistant *Staphylococcus aureus*, or *Acinetobacter baumannii*. The study

Editor Mariana Castanheira, JMI Laboratories

Copyright © 2022 Di Blasio et al. This is an open-access article distributed under the terms of the [Creative Commons Attribution 4.0 International license](https://creativecommons.org/licenses/by/4.0/).

Address correspondence to A. James Mason, james.mason@kcl.ac.uk.

The authors declare no conflict of interest.

Received 14 October 2022

Accepted 18 November 2022

Published 13 December 2022

provides a rationale for further adaptation toward diversifying the range of indications in which this class of antimicrobial may be used.

KEYWORDS dequalinium chloride, synergy, aminoglycosides, *Galleria mellonella*

The stark prediction of the 2016 Review on Antimicrobial Resistance (1), that around 10 million deaths per year will be attributable to antimicrobial resistance (AMR) by the year 2050, has been reinforced by the recent finding that more than 1.2 million deaths in 2019 were a direct result of antibiotic-resistant bacterial infections (2). Actions recommended by the 2016 review to avert this include (i) identifying new antimicrobials that are effective against emerging drug-resistant bacteria and (ii) adopting more appropriate use of existing antimicrobials so their utility endures longer. Consistent with these two principles is the modification of existing antimicrobials to extend their range of applications and/or to mitigate the risk of resistance developing.

Bolaamphiphiles are amphipathic molecules that are composed of two hydrophilic groups at either end of an interconnecting hydrophobic skeleton chain (3). Notable examples from nature include lipids from archaeobacteria, which form monolayered membranes, and, from the clinical setting, dequalinium chloride (DQC). DQC is composed of two quaternary quinolinium groups attached at either end of an *N*-decylene chain. It is available as throat lozenges (Dequadin) for treatment of sore throat and also thrush and glossitis, both notably associated with candidiasis, and is indicated for use as a topical treatment for bacterial vaginosis, formulated in tablets that are inserted at night (Fluomizin) (4). While DQC inhibits protein kinase C and is toxic toward mitochondria, it has many attractive features, including antibacterial, antifungal, antimalarial, and antitrypanosomal activity, while it is also an inhibitor of mycothiol ligase in *Mycobacterium tuberculosis* (5–7). Therefore, if the limitations that currently restrict the application of DQC can be better understood and overcome, there is scope for wider application of this class of antimicrobial.

12,12'-(Dodecane-1,12-diyl)-bis-(9-amino-1,2,3,4-tetrahydroacridinium) chloride (12-bis-THA Cl₂, referred to here as CM2), was developed from a group of compounds, themselves developed by Weissig et al. from DQC (8), that varied in their self-assembly properties (9). Of these, 10-bis-THA, which includes a primary amine and bulky aliphatic residue in the headgroup and which was prepared as an iodide salt, formed the smallest vesicles with a narrow size distribution. Replacing iodide with chloride improves solubility and also self-assembly, and increasing the length of the interconnecting acyl chain from 10 to 12 carbons produced CM2, which has been used as an oligonucleotide nanovector (9). However, the CM2 headgroup, tacrine, is able to intercalate into DNA and is a topoisomerase inhibitor (10). Further development of CM2 toward use as an antimicrobial therefore hinges on evaluating the impact of its increased hydrophobicity and propensity to self-associate, relative to DQC, as well as investigating whether and how its intercalation and other undesirable properties may be mitigated.

Here, we describe a structure-activity relationship (SAR) approach that seeks to obtain a better understanding of the properties of cationic bolalipids that affect their antimicrobial activity and their potential to be used in a broader range of health care settings. The SAR study used CM2 as a starting point, and we investigated the ability of a series of analogues, with more or less bulky headgroups or with shorter acyl chains, to intercalate in DNA, their *in vitro* antibacterial and antifungal activities—including how synergy with existing antibiotics may alter their pharmacodynamic (PD) profile—and how the determinants of *in vitro* activity vary between microbial targets and also differ for successful therapy in *Galleria mellonella* infection models.

RESULTS

Analogue design and synthesis. Because of the overarching aim to see if DNA intercalation and topoisomerase inhibition can be reduced while maintaining antimicrobial activity, seven new bolalipid analogues (Fig. 1C to I) were designed in which the bulkiness and planarity of the headgroup and/or the length of the acyl linker were varied. Each of these

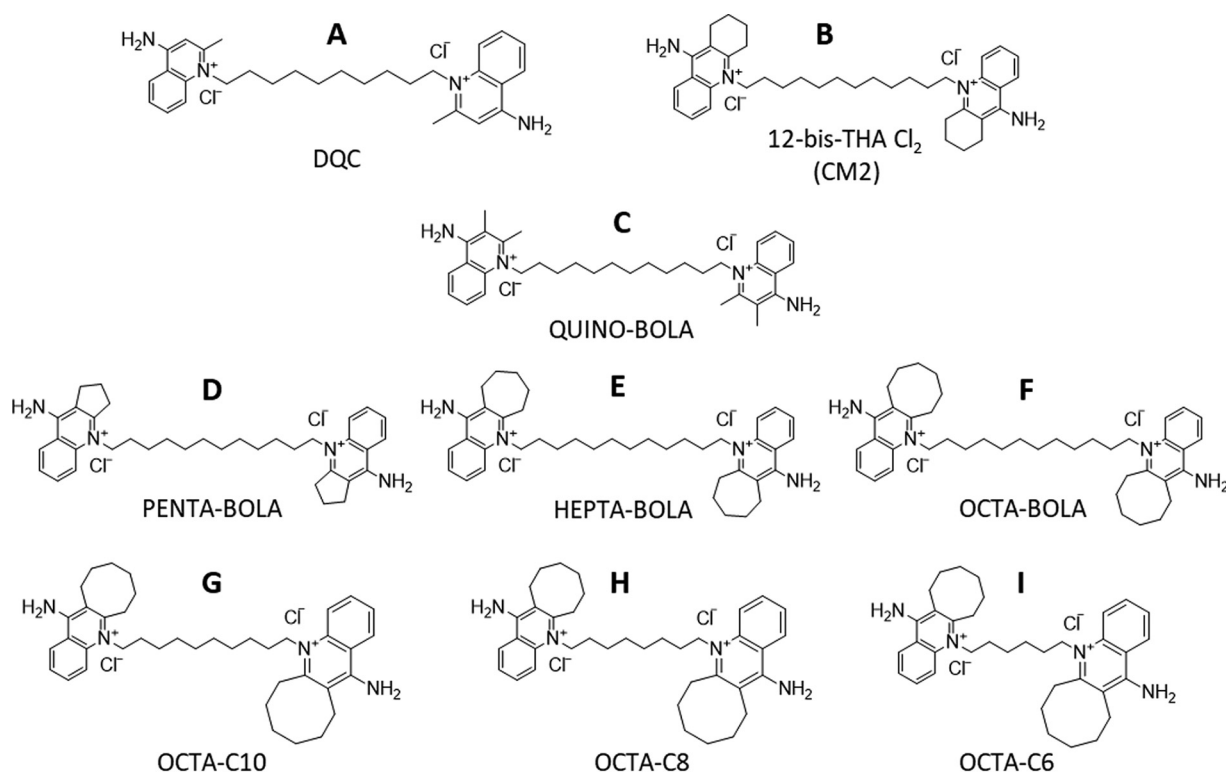


FIG 1 Design and naming of 12-bis-THA Cl₂ analogues. Dequalinium chloride (A), CM2/12-bis-THA Cl₂ (B), and the new bolalipids Quino-bola (C), Penta-bola (D), Hepta-bola (E), Octa-bola (F), Octa-C10 (G), Octa-C8 (H), and Octa-C6 (I), all prepared as chloride salts.

changes also impacts the overall hydrophobicity of the bolalipid, though the impacts of increasing the hydrophobicity of the headgroup or linker may differ. Starting with CM2 (Fig. 1B), the aliphatic region of the headgroup is either shrunk to from a six-carbon ring to either a five-carbon ring (Penta-bola) (Fig. 1D) or just two methyl groups (Quino-bola) (Fig. 1C) or enlarged to seven-carbon (Hepta-bola) (Fig. 1E) or eight-carbon (Octa-bola) (Fig. 1F) rings, which are bulkier and further disrupt the planarity of the headgroup. The rationale behind this strategy is based on the presence of free rotation around the N⁺-C bond: the bulky headgroups could be oriented in a way that could obstruct the headgroup and prevent it from inserting into DNA, whereas a less bulky one could facilitate the headgroup insertion between two successive DNA base pairs. Each of these analogues has the same twelve-carbon acyl linker.

Analogues with shorter acyl chains (Fig. 1G to I) compensate for the enlargement of the aliphatic region of the headgroup, which increases the overall hydrophobicity of the Octa-bola molecule relative to CM2. These analogues have either 10-carbon (Octa-C10) (Fig. 1G), eight-carbon (Octa-C8) (Fig. 1H), or six-carbon (Octa-C6) (Fig. 1I) acyl linkers.

Synthesis of the bolalipids is described in detail in the supplemental material. The four new headgroups were prepared with yields ranging from 45% (Penta) to 94% (Quino), and these compare favorably with tacrine, which in our hands was prepared at a yield of 61%. However, and as might be expected from previous studies of synthesis of gemini (*twin*) compounds based on either 4-aminopyridinium or 4-aminoquinolinium headgroups (11), the tricyclic system may reduce the endocyclic nitrogen reactivity, and this is consistent with the relatively low yields (5 to 10%) obtained for the final bolalipids. Ion exchange was used to replace iodide and obtain the bolalipids as chloride salts.

Increasing bolalipid headgroup bulkiness and shortening acyl linker reduces intercalation and topoisomerase I inhibition. The DNA unwinding assay is sensitive to topoisomerase inhibition and is a measure of DNA intercalation potential. While

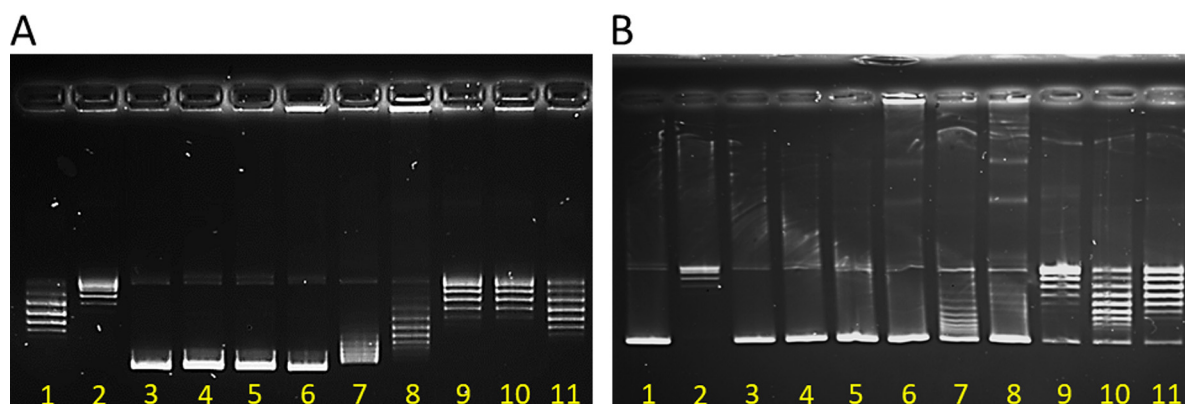


FIG 2 DNA intercalation is prevented by increasing bulkiness of the bolalipid headgroup. Unwinding assay gels are shown for relaxed (A) and supercoiled (B) pBR322 plasmid. In both gels, lane 1 contains plasmid only and lanes 2 to 11 contain plasmid plus topoisomerase I either alone (lane 2) or with DQC (lane 3), Quino-bola (lane 4), Penta-bola (lane 5), CM2 (lane 6), Hepta-bola (lane 7), Octa-bola (lane 8), Octa-C10 (lane 9), Octa-C8 (lane 10), or Octa-C6 (lane 11). Gel images were sharpened and brightness and contrast were enhanced to enable all bands to be discerned.

fluoroquinolones such as ciprofloxacin inhibit topoisomerase activity and intercalation into genomic and/or mitochondrial DNA may contribute to antimicrobial activity, the DNA unwinding assay is used here primarily as a measure of relative risk of genotoxicity. The relaxed pBR322 plasmid migrates as at least five separate bands during electrophoresis, representing multiple topoisomers (Fig. 2A, lane 1). Upon treatment with topoisomerase I, the plasmid is concentrated into one or two bands and does not migrate as far, as the preferred topoisomers are produced (Fig. 2A, lane 2). DQC, Quino-bola, Penta-bola, CM2 and, to a slightly lesser extent, Hepta-bola are intercalators and may also interfere with the action of the enzyme (Fig. 2A, lanes 3 to 7). In contrast, the larger-headgroup bolalipid, Octa-bola, has less of an impact and, while it may inhibit the activity of topoisomerase I, its intercalation is reduced if not eliminated (Fig. 2A, lane 8). Reducing the length of the acyl chain linker for the Octa analogues further reduces the intercalation and may mitigate the enzyme inhibition (Fig. 2A, lanes 9 to 11). The supercoiled plasmid is relaxed through the action of topoisomerase I (Fig. 2B, lanes 1 and 2). This effect is not observed when any of DQC, Quino-bola, Penta-bola, CM2, Hepta-bola, or Octa-bola is also present (Fig. 2B, lanes 3 to 8). Only when the acyl linker is shortened in further Octa analogues is some relaxed plasmid observed, though this effect is again impaired (Fig. 2B, lanes 9 to 11).

Relationship of structure to antimicrobial activity. The antimicrobial activities of DQC, CM2 and the new bolalipid analogues were tested against a panel of Gram-negative and Gram-positive bacteria, *Candida* spp., and mycobacteria (Tables 1, 2, and 3). As a class, the bolalipids are all more active against Gram-positive species, *Candida* spp., and both *Mycobacterium smegmatis* mc² 155, and *M. tuberculosis* Bleupan than against Gram-negative species. CM2 is a little more potent than DQC against the Gram-negative species, *Candida* spp., and mycobacteria, but it outperforms DQC by an order of magnitude or more against the Gram-positive bacteria. Variation in activity across CM2 and the new bolalipids is modest, but Octa-bola is consistently found to be the most potent of the analogues, and both it and Octa-C10 have notably improved activity against *Escherichia coli* and *Acinetobacter baumannii*. All the bolalipids have substantial *in vitro* toxicity, with half-maximal effective concentrations (EC₅₀) ranging from only 3.5 μ g/mL to 34.7 μ g/mL against either HEK293 or HeLa cells for bolalipids with 12- or 10-carbon acyl linkers.

Despite this, an *in vitro* selectivity index of 23.9 suggests that Octa-C10 might have potential to be developed as a therapeutic for Gram-positive bacterial infections, and it modestly outperforms DQC against bacteria associated with bacterial vaginosis, i.e., Gram-variable *Gardnerella vaginalis* and Gram-negative *Prevotella bivia* (Table 4). In contrast, the *in vitro* data suggest that none of the bolalipids are suitable candidates for

TABLE 1 MICs of bolaamphiphiles against a panel of Gram-positive and Gram-negative bacteria, *Candida* spp., and mycobacteria

Category and organism	MIC (µg/ml) of ^a :									
	12-bis-THA Cl ₂	Dequalinium	Quino-bola	Penta-bola	Hepta-bola	Octa-bola	Octa-C10	Octa-C8	Octa-C6	Fluconazole
Gram-negative bacteria										
<i>Klebsiella pneumoniae</i> NCTC 13368	32	>32	32	32	32	32	32	32	>32	>32
<i>Klebsiella pneumoniae</i> M6	16	>32	32	32	16	16	16	16	>32	>32
<i>Acinetobacter baumannii</i> AYE	16	32	32	32	16	8	16	32	>32	>32
<i>Acinetobacter baumannii</i> ATCC 17978	16	32	16	16	16	8	32	32	>32	>32
<i>Pseudomonas aeruginosa</i> PAO1	32	>32	>32	32	32	32	>32	>32	>32	>32
<i>Pseudomonas aeruginosa</i> NCTC 13437	32	>32	>32	>32	32	32	>32	>32	>32	>32
<i>Escherichia coli</i> NCTC 12923	4	32	8-16	16	2	2	2	2	>32	>32
Gram-positive bacteria										
EMR <i>Staphylococcus aureus</i> 15 NCTC 13616	0.25	8	1	0.5	0.25	0.125	0.25	0.25	1	16
EMR <i>Staphylococcus aureus</i> 16 NCTC 13277	0.125	4	1	0.5	0.25	0.125	0.25	0.25	1	16
VS <i>Enterococcus faecalis</i> NCTC 775	2	32	4	4	1	0.5	2	2	4	32
VR <i>Enterococcus faecalis</i> NCTC 12201	1	16	2	1	0.5	1	1	1	4	16
VR <i>Enterococcus faecium</i> NCTC 12204	0.5	8	2	1	0.5	0.5	0.25	0.25	0.5	16
Fungi										
<i>C. albicans</i> 3179	0.25	0.5	0.25	0.25	0.5	0.5	0.5	0.5	2	8
<i>C. albicans</i> 3281	0.25	0.5	0.25	0.25	0.5	0.5	0.5	1	2	>128
<i>C. auris</i> temp probe	2	4	2	2	2	1	4	4	4	>8
<i>C. glabrata</i> 8018	0.25	0.5	0.25	0.25	0.25	0.5	0.5	0.5	2	>8
<i>C. tropicalis</i> 8760	0.25	0.5	0.25	0.25	0.25	0.25	0.25	0.25	1	8
<i>C. krusei</i> 3876	0.5	1	1	0.5	0.5	0.5	2	2	4	32
<i>C. parapsilosis</i> 3209	1	4	0.5-2	1	1	0.5	2	2	4	>8
<i>C. parapsilosis</i>	2	8	2	1	2	1	4	4	8	0.5
Mycobacteria										
<i>M. smegmatis</i> mc ² 155	0.28	0.68	0.49	0.10	ND	0.55	ND	ND	0.19	1.66
<i>M. tuberculosis</i> Bleupan	0.87	3.51	ND	0.19	ND	0.24	ND	ND	0.49	0.46

^aBold indicates the best bolaamphiphile. VR, vancomycin resistant; VS, vancomycin susceptible; ND, not determined.

TABLE 2 Toxicity of bolaamphiphiles for two cell lines^a

Cell line	Toxicity (EC ₅₀ [μ g/ml]) of:								
	12-bis-THA Cl ₂	Dequalinium	Quino-bola	Penta-bola	Hepta-bola	Octa-bola	Octa-C10	Octa-C8	Octa-C6
HEK293	5.5 \pm 2.0	9.9 \pm 3.3	13.6 \pm 0.6	7.9 \pm 1.2	3.5 \pm 1.2	3.8 \pm 0.3	7.0 \pm 0.5	12.9 \pm 4.3	40.0 \pm 15.6
HeLa	7.1 \pm 2.0	34.7 \pm 13.9	13.9 \pm 9.5	9.5 \pm 1.7	4.5 \pm 0.7	4.5 \pm 0.7	10.7 \pm 0.3	27.3 \pm 1.3	64.3 \pm 3.6

^aAverage \pm standard error from 3 independent repeats. Bold indicates the best bolaamphiphile.

development for infections caused by other Gram-negative bacteria, at least when used alone.

In contrast to Gram-positive bacteria, where the greater *in vitro* selectivity indices are found for bolalipids with larger headgroups, the most attractive *in vitro* selectivity indices for *Candida* spp. are found for bolalipids with the smaller headgroups, with Quino-bola being only marginally better than DQC. The *in vitro* toxicity of the Octa analogues decreases as the acyl linker is shortened, and since the potency against *M. tuberculosis* Bleupan both is high and does not vary substantially across the tested bolalipids, Octa-C6 is found to have an attractive *in vitro* selectivity index with 2 orders of magnitude difference between active and toxic concentrations.

The very different distribution of selectivity indices, according to the target microbial species, highlights the fact that the antimicrobial activity against Gram-negative and Gram-positive bacteria, *Candida* spp., and mycobacteria is underpinned by different properties. To explore this further and consider the role of hydrophobicity, which is altered as a result of the modifications in the SAR, the toxicity to mammalian cells (Fig. 3A and B), potency against *Candida albicans* (Fig. 3C and D), and representative Gram-negative (Fig. 3E) or Gram-positive (Fig. 3F) bacteria were plotted as a function of the calculated partition coefficient (c -logP).

For the Octa- series, in all cases, both the toxicity and antimicrobial potency decreased as the acyl linker was shortened and the hydrophobicity and partition coefficient decreased (Fig. 3A to F). Similarly, if headgroup modifications alone are considered (for twelve-carbon bolalipids), as the hydrophobicity and partition coefficient decrease, so does the toxicity to mammalian cells (Fig. 3A and B) and potency against bacteria (Fig. 3E and F). In contrast however, the opposite is true of potency toward *C. albicans* (Fig. 3C and D). Here, bolalipids with a lower hydrophobicity and partition coefficient are more potent, and these are also the bolalipids that are strong intercalators per the unwinding assay discussed above. Notably, we could detect accumulation of Penta-bola in *Candida auris* TGD1912 at a concentration more than 50 times the MIC without any evidence of plasma membrane damage (see Fig. S1 in the supplemental material); similar behavior for CM2 accumulating in *Pseudomonas aeruginosa* PAO1 is described below.

Bolalipids act in synergy with aminoglycosides against *P. aeruginosa*, with the combinations being more bactericidal. The antibacterial activity of the bolalipids was investigated in combination with antibiotics relevant to clinical or veterinary practice. In screening, using a fixed (0.25 \times MIC) concentration of Octa-bola, Octa-C10, or Octa-C6, we found consistent potentiation of both tobramycin and gentamicin antibacterial activities against both sensitive and aminoglycoside-resistant strains of *A. baumannii* and *P. aeruginosa* but not *E. coli* or *Klebsiella pneumoniae* (Table 5). Using checkerboard assays, we confirmed that strong synergy is observed between the aminoglycoside tobramycin and bolalipids against *P. aeruginosa* (Table 6). This was observed irrespective of the potency of the

TABLE 3 Selectivity indices of bolaamphiphiles

Organism	Selectivity of ^a :								
	12-bis-THA Cl ₂	Dequalinium	Quino-bola	Penta-bola	Hepta-bola	Octa-bola	Octa-C10	Octa-C8	Octa-C6
Gram-negative bacteria (avg)	0.48	0.69	0.55	0.35	0.44	0.53	1.07	0.90	<1.63
Gram-positive bacteria (avg)	19.5	2.65	8.94	10.9	10.4	17.4	23.9	18.1	2.94
Fungi (avg)	15.8	26.8	31.8	22.3	8.00	8.30	11.6	8.48	<6.52
<i>M. tuberculosis</i> Bleupan	7.24	6.35	ND	45.8	ND	17.3	ND	41.0	113

^aRatio of average toxicity (HEK293 and HeLa) to average potency. Bold indicates the best bolaamphiphile. ND, not determined.

TABLE 4 MICs of DQC and Octa-C10 against a panel of *G. vaginalis* isolates and *P. bivia* NCTC 11156

Organism	MIC ($\mu\text{g/mL}$) ^a	
	DQC	Octa-C10
<i>Prevotella bivia</i> NCTC 11156	2	0.125
<i>G. vaginalis</i> NCTC 10287	2	0.5–1
<i>G. vaginalis</i> KC1	2	0.5–1
<i>G. vaginalis</i> KC2	4	2
<i>G. vaginalis</i> KC3	2–4	0.5

^aSelectivity indices (ratio of average toxicity [HEK293 and HeLa] to average potency) were 8.58 and 10.7 for DQC and Octa-C10, respectively.

bolalipid alone; synergy was observed for DQC, Quino-bola, and Octa-C6, which all have relatively low antibacterial activities. Again, strong synergy was also observed for *P. aeruginosa* isolates that either have reduced sensitivity to tobramycin (RP73) or are resistant (NCTC 13437). However, the synergy observed between bolalipids and aminoglycosides against *A. baumannii* and *P. aeruginosa* does not extend to other species or other antibiotics (Tables S1 and S2).

There was no synergy between Octa-bola or Octa-C10 and a range of antibiotics against either antibiotic-sensitive or -resistant *P. aeruginosa*. As has been observed previously for DQC, which induces expression of the efflux pump MexCD-OprJ (12), antagonism is consistently observed between both Octa-bola and Octa-C10 and ciprofloxacin, a fluoroquinolone which acts by inhibiting DNA topoisomerases (Table S1). Synergy between Octa-C10 and streptomycin against *Actinobacillus pleuropneumoniae* isolates was modest (Table S2). In addition, while modest synergy was observed between Octa-C10 and enrofloxacin against some *Ac. pleuropneumoniae* isolates (Fig. S2), there was no effect of combining Octa-C10 and amoxicillin. Synergy was also tested between Octa-C10 and vancomycin, clindamycin, or linezolid against epidemic methicillin-resistant *Staphylococcus aureus* 15 (EMRSA-15), where the effect was additive, and there was no effect of combining Octa-C10 and rifampin against EMRSA-15.

To better understand the potential mechanism of synergy between the bolalipids and tobramycin against *P. aeruginosa*, we investigated the ability of DQC and CM2 to damage models of bacterial plasma membranes (Fig. S2) and the ability of CM2 to accumulate within bacteria (Fig. 4A and B). We have developed a patch-clamp approach to study the concentration-dependent effect of antimicrobial peptide (AMP) challenge on models of bacterial plasma membranes (13–15). In this approach, we identify the lowest antimicrobial concentration that induces conductance and then study the membrane activity at this concentration. For AMPs that are supposed to have a predominantly membrane disruptive mechanisms of activity, it is common for conductance to be induced at concentrations between 5 and 10 μM (13, 14), and sometimes as low as 2.5 μM (15). In contrast, 90 μM DQC or CM2 is required to induce any conductance in bilayers composed of DiPhytanoyl PhosphatidylGlycerol (DPhPG) (Fig. S2).

The red-shifted fluorescence emission spectrum of CM2 relative to DQC (Fig. S3) enables its detection by fluorescence microscopy using a filter commonly used to detect Hoechst 33258. When *P. aeruginosa* PAO1 was challenged with 180 μM CM2, i.e., twice the concentration that induces conductance in the patch-clamp experiments, the bacteria appeared intact and the bolalipid was concentrated within the cells (Fig. 4A). The same behavior was observed when the same treatment was performed in the presence of subinhibitory concentrations of tobramycin (Fig. 4B). Next, we compared the *in vitro* pharmacodynamic behavior of tobramycin alone with that observed when a bolalipid was added in combination. Aminoglycosides such as tobramycin are weakly bactericidal, and we investigated whether the substantial synergistic increase in potency, obtained by combining tobramycin with Octa-bola, might be associated with changes in *in vitro* pharmacodynamic properties (Fig. 4). Although, on average, the most synergy between bolalipids and

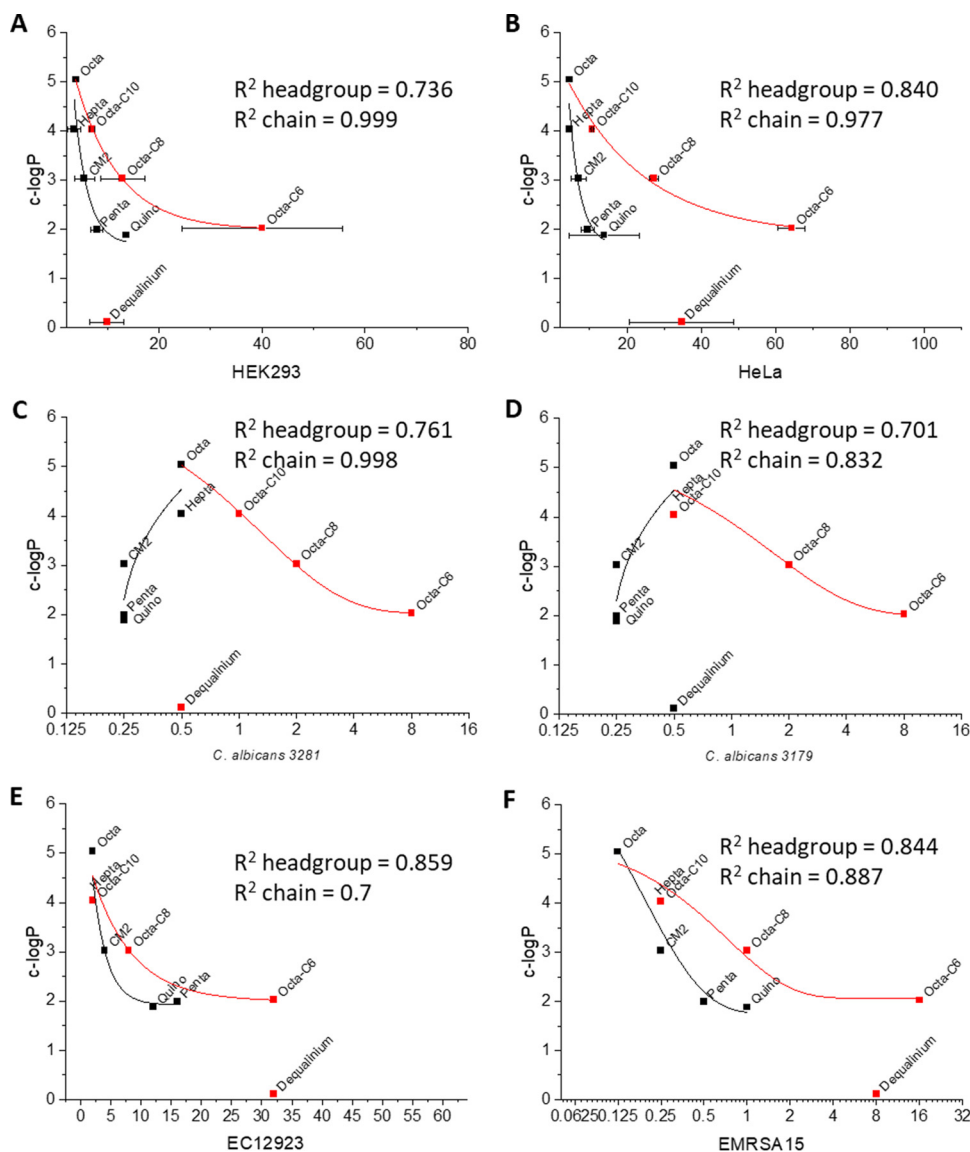


FIG 3 Bolaamphiphiles have a distinct mechanism when targeting fungal pathogens. Toxicity for mammalian cells (EC_{50}) (A and B), MICs against *C. albicans* (C and D) or representative Gram-negative (*E. coli* 12923) (E) and Gram-positive (EMRSA-15) bacteria (F) (all in micrograms per milliliter) were plotted as a function of calculated logP. Exponential decay fits were used for all headgroup and chain SARs except for the headgroup for *C. albicans*.

tobramycin is found with a bolalipid/aminoglycoside ratio of 13:1 (wt/wt), we opted to use a ratio of only 2:1 to test whether only a little bolalipid can affect the PD.

The cooperativity of the dose-dependent activity, as characterized by the steepness of the slope in a dose-response curve and the parameter kappa, was unaffected by the addition of the bolalipid, and this parameter was similar under all conditions tested (Fig. 4C and E). As evidenced by the minimum growth rate (ψ_{\min}), tobramycin and colistin are both weakly bactericidal against *P. aeruginosa* RP73 (Fig. 4C and D), but the combination of Octa-bola and tobramycin killed at a much higher rate than either colistin or tobramycin alone ($P < 0.0001$). Insufficient material precluded assessment of bactericidal activity above $100 \times$ MIC ($800 \mu\text{g}/\text{mL}$); however, Octa-bola was also seen to be strongly bactericidal, albeit only at the highest concentration tested. Taken together, these experiments show that the combination of bolalipids and tobramycin increases the overall potency and bactericidal rate against *P. aeruginosa*. This was

TABLE 5 Synergy between bolalipids and aminoglycosides for two Gram-negative species

Strain	MIC ($\mu\text{g/mL}$) of ^a :							
	Tobramycin				Gentamicin			
	No bola	Octa-Bola	Octa-C10	Octa-C6	No bola	Octa-Bola	Octa-C10	Octa-C6
<i>K. pneumoniae</i> NCTC 13368	8	4	8	16	16	8	16	16
<i>K. pneumoniae</i> M6	1	0.5	0.25	1	1	1	1	1
<i>A. baumannii</i> AYE	64	8	4	16	256	0.5	4	32
<i>A. baumannii</i> ATCC 17978	2	0.125	0.5	0.5	2	0.25	1	1
<i>P. aeruginosa</i> PAO1	1	0.5	0.25	0.5	2	0.5	0.25	0.25
<i>P. aeruginosa</i> NCTC 13437	64	8	4	8	256	8	8	8
<i>E. coli</i> NCTC 12923	2	1	1	2	2	2	1	2

^aBroth microdilution assay results for a panel of Gram-negative bacterial strains challenged with antibiotic in the presence of fixed concentrations ($0.25 \times \text{MIC}$) of the indicated bolalipids. Values in bold represent a ≥ 2 -dilution increase in aminoglycoside potency and hence an FIC of ≤ 0.5 , considered to indicate strong synergy.

achieved without disrupting the bacterial plasma membrane but while bolalipids penetrated the bacteria cytoplasm.

Shortening the chain of Octa-bola improves *in vitro* selectivity but impairs therapy. According to the *in vitro* selectivity indices described above, Octa-C10 and Octa-C6 were selected for evaluation in intrahemocoelic *Galleria mellonella* models of, respectively, EMRSA-15 (Fig. 5) and *M. tuberculosis* Bleupan (Fig. 6) infection. *G. mellonella* responded to treatment of an EMRSA-15 infection with vancomycin in a dose-dependent manner (Fig. 5A). Vancomycin at 50 mg/kg rescued almost 80% of infected *G. mellonella* larvae ($P < 0.0001$), while a tenth of this dose was moderately less effective, rescuing 45% of infected larvae ($P < 0.001$). In the same model, the lowest dose of Octa-C10, 0.1 mg/kg, rescued approximately a third of the infected larvae ($P = 0.0167$; log rank [Mantel-Cox] test) (Fig. 5B). However, increasing the dose did not lead to further protection, and, indeed, higher doses performed worse, with none of them providing significant protection (Fig. 5B).

All *G. mellonella* larvae were rescued from *M. tuberculosis* Bleupan infection by 10 mg/kg rifampin (Fig. 6A). Treatment with Octa-C6, however, did not provide protection, and indeed, survival was significantly worse when the three lower doses (0.01, 0.1, and 1 mg/kg) were administered (Fig. 6B). A dose of 0.1 mg/kg DQC also led to lower survival in this model, though the survival of larvae was indifferent to treatment with higher or lower doses (Fig. 6C). In contrast with the results observed with Octa-C6, treatment with the more hydrophobic Octa-bola did not lead to worse survival and survival improved following treatment with intermediate doses, with 1 mg/kg Octa-bola rescuing about half of the infected larvae ($P = 0.0316$; log rank [Mantel-Cox] test) (Fig. 6D).

To better understand factors that might affect *in vivo* performance, we conducted dynamic light scattering (DLS) measurements to measure the relative propensity of

TABLE 6 Tobramycin acts in synergy with bolalipids against *P. aeruginosa*^a

Combination	Strain	MIC ($\mu\text{g/mL}$)				
		Alone		In combination		FIC
		Bolalipid	Antibiotic	Bolalipid	Antibiotic	
DQC-tobramycin	<i>P. aeruginosa</i> PAO1	>32	0.5	8	0.25	<0.75
Quino-bola-tobramycin	<i>P. aeruginosa</i> PAO1	>32	0.5	8	0.0625	<0.375
Penta-bola-tobramycin	<i>P. aeruginosa</i> PAO1	32	0.5	8	0.0625	0.375
CM2-tobramycin	<i>P. aeruginosa</i> PAO1	32	0.5	4	0.0625	0.25
Hepta-bola-tobramycin	<i>P. aeruginosa</i> PAO1	32	0.5	8	0.125	0.5
Octa-bola-tobramycin	<i>P. aeruginosa</i> PAO1	32	0.5	4	0.125	0.375
Octa-C10-tobramycin	<i>P. aeruginosa</i> PAO1	64	0.5	16	0.125	0.5
	<i>P. aeruginosa</i> RP73	8	2	1	0.25	0.25
	<i>P. aeruginosa</i> NCTC 13437	32	64	8	4	0.3125
Octa-C6-tobramycin	<i>P. aeruginosa</i> RP73	64	2	4	0.125	0.0625

^aConcordant results from two or more independently repeated experiments are shown.

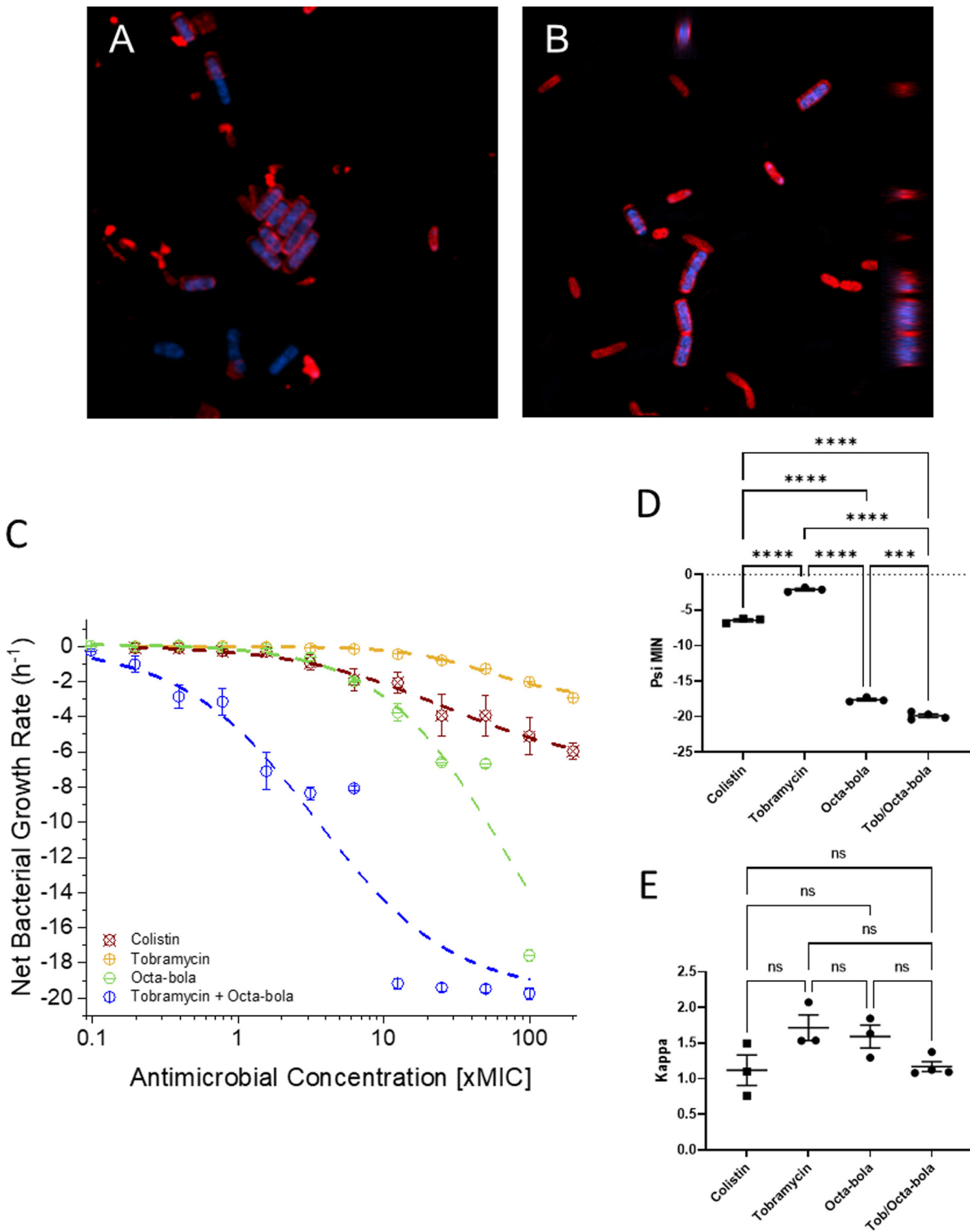


FIG 4 Synergistic activities of bolalipids with tobramycin against *P. aeruginosa*. Penetration of CM2 into *P. aeruginosa* PAO1. Bacteria were challenged with $180 \mu\text{M}$ CM2 in the absence (A) or (B) presence of tobramycin. Red staining represents WGA 555 (wheat germ agglutinin bound to tetramethylrhodamine), while the intrinsic fluorescence of CM2 appears blue. Images were taken 75 min postadministration. (C to E) Pharmacodynamic response of *P. aeruginosa* RP73 challenged with increasing concentrations of colistin, tobramycin, Octa-bola, or a 2:1 (wt/wt) combination of tobramycin and Octa-bola. The curves are fits of averages from three independent repeated experiments (C). One-way ANOVA with Tukey's *post hoc* test multiple comparisons for psi-min (D) and kappa (E) highlights the differences in bactericidal rate but not cooperativity between the conditions. ns, $P > 0.05$; ***, $P < 0.001$; ****, $P < 0.0001$.

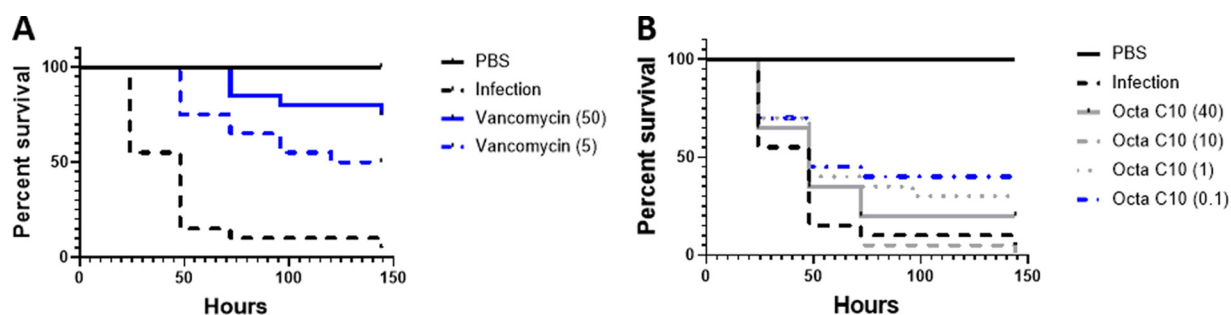


FIG 5 Octa-C10 bolalipid dose determines therapeutic outcomes in an intrahemocoelic *G. mellonella* model of EMRSA-15 infection. Survival curves for 20 TruLarv larvae are shown for different doses (in milligrams per kilogram) of vancomycin (A) or Octa-C10 (B). Treatment curves that differ ($P < 0.05$) with respect to infection only by log rank (Mantel-Cox) tests are shown in blue.

bolalipids to form nanoparticles as an indicator of their tendency to aggregate (Table S3). Of the longer-chain bolalipids, Octa-bola and DQC had the greatest ability to form nanoparticles, followed by CM2 and Penta-bola, with Quino-bola showing the least ability to form nanoparticles. Under no conditions did Octa-C6 give evidence of nanoparticle formation.

Since none of the bolalipids were toxic to *G. mellonella* in the absence of infection, we conclude that, in the *M. tuberculosis* Bleupan infection model and possibly in the EMRSA-15 infection model, bolalipids can act to exacerbate the infection. Since this is not linearly related to dose and the greatest exacerbation was observed for the most soluble bolalipid, Octa-C6, it is apparent that *in vitro* toxicity profiles and selectivity indices may not predict *in vivo* performance.

Longer-chain bolalipids are effective therapeutics in models of *Escherichia coli* ATCC 25922 infection. Despite the poor *in vitro* toxicity profile and selectivity indices of the twelve-carbon bolalipids, we evaluated whether they may nevertheless provide protection *in vivo* in an intrahemocoelic *G. mellonella* model of *E. coli* ATCC 25922 infection. The *in vitro* selectivity indices of the twelve-carbon bolalipids for Gram-negative bacteria are broadly similar, and where antibacterial potency is low, there are corresponding reductions in cytotoxicity, notably for Quino-bola and DQC. Unlike with *M. tuberculosis* Bleupan, DQC was protective in *G. mellonella* against *E. coli* ATCC 25922 infection (Fig. 7). DQC performed significantly better than Quino-bola ($P = 0.041$, Gehan-Breslow-Wilcoxon test; $P > 0.05$, log rank [Mantel-Cox] test) (Fig. 7A), and neither Quino-bola nor Penta-bola offered significant protection. Other bolalipids, including Hepta-bola (Fig. 7C) and Octa-bola (Fig. 7D), were also significantly protective and were not significantly worse than DQC. The performance of CM2 was between that of the bolalipids with larger and smaller headgroups (Fig. 7), and survival was somewhat better than that obtained in the absence of treatment ($P = 0.0527$, log rank [Mantel-Cox] test).

Finally, we assessed whether a combination of Octa-bola and tobramycin or of Octa-C10 and gentamicin might be protective in *G. mellonella* models of intrahemocoelic *Pseudomonas aeruginosa* RP73 or *Acinetobacter baumannii* ATCC 17978 burn wound infections, respectively. *G. mellonella* larvae are very sensitive to intrahemocoelic infection with *P. aeruginosa*, and both 1×10^2 CFU and 1×10^1 CFU per larva induced substantial mortality after 96 h (65% and 43%, respectively). Tobramycin at 50 mg/kg rescued 97.5% of the larvae infected with the higher dose ($P < 0.0001$, log rank [Mantel-Cox] test), while 5 mg/kg tobramycin rescued 37.5% of the larvae ($P = 0.0084$). Addition of 0.25, 1, 4, or 10 mg/kg Octa-bola to 5 mg/kg tobramycin did not improve larva rescue; indeed, the lowest Octa-bola dose impaired the therapy formerly attributed to the tobramycin ($P = 0.0049$) but did not exacerbate the infection.

While *G. mellonella* can tolerate superficial burns, subsequent infection with *A. baumannii* ATCC 17978 led to 62.5% mortality in 96 h ($P < 0.0001$, log rank [Mantel-Cox] test), allowing effective therapy to be quantified (Fig. 8). In a dose-response experiment, 5 mg/kg gentamicin was protective ($P < 0.0001$), with 76% larvae rescued, but

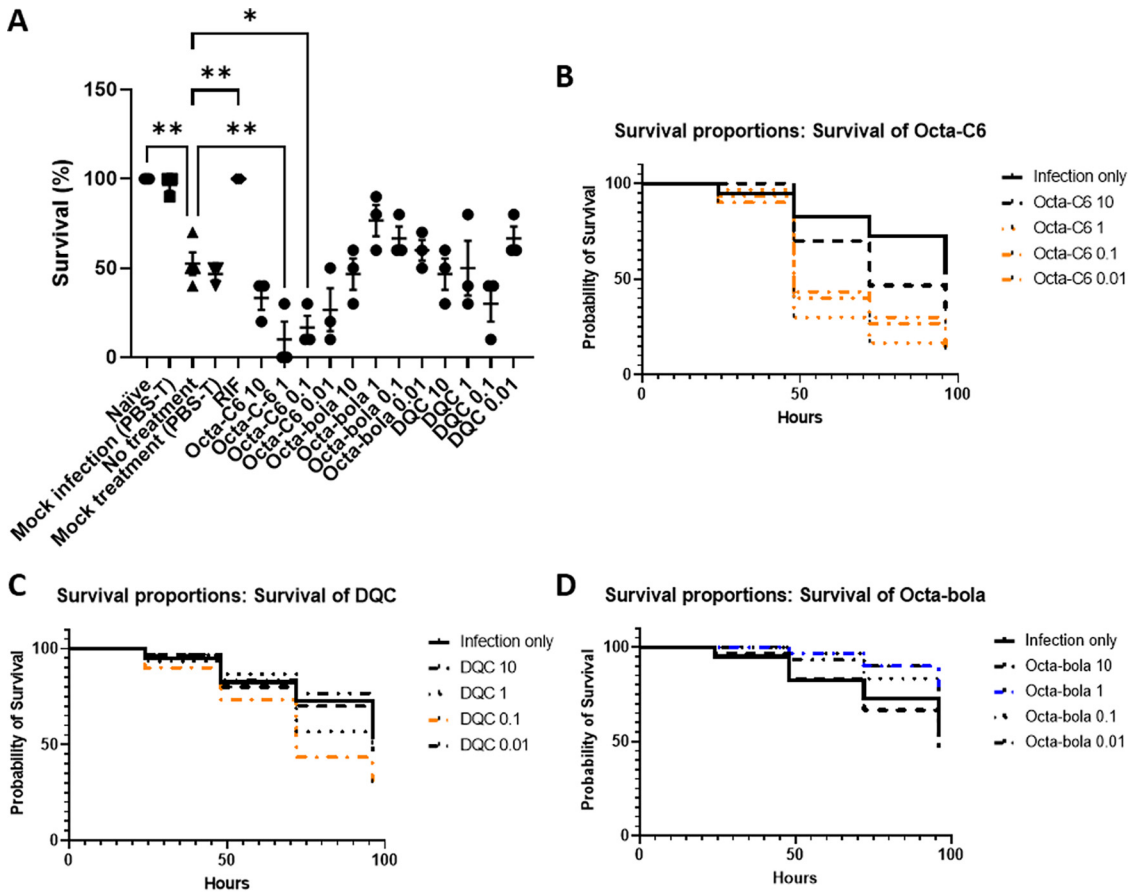


FIG 6 Bolalipid chain length determines therapeutic outcomes in a *G. mellonella* model of *M. tuberculosis* Bleupan infection. (A) Survival of 10 TruLarv larvae after 96 h, each treated with the indicated bolalipids (doses are in milligrams per kilogram). Rifampin (RIF; 10 mg/kg) and PBS-T were used as positive and negative controls, respectively. Data were obtained in three independent repeats, and significance is shown relative to the no-treatment value with Dunnett’s correction for multiple comparisons applied. *, $P < 0.05$; **, $P < 0.01$. (B to D) Survival curves for 30 TruLarv larvae for different doses (in milligrams per kilogram) of Octa-C6 (B), DQC (C), and Octa-bola (D). Curves that differ ($P < 0.05$) with respect to infection only by either log rank (Mantel-Cox) or Gehan-Breslow-Wilcoxon tests are shown in orange (exacerbation) or blue (protection).

lower doses (2.5 and 1.25 mg/kg) were ineffective (Fig. 8A). When used alone, Octa-C10 was also protective in this model, with doses of 10 and 5 mg/kg rescuing 60% ($P = 0.0002$) and 48% ($P = 0.0042$) of the larvae, respectively, but lower doses (2.5 and 1.25 mg/kg) being ineffective (Fig. 8B). When combinations were used to assess *in vivo* synergism, a low dose of gentamicin (2.5 mg/kg) was protective in combination with doses of 2.5 mg/kg Octa-C10 and above (Fig. 3C), rescuing 44% (2.5 mg/kg; $P = 0.0072$), 40% (5 mg/kg; $P = 0.0211$), and 64% (10 mg/kg $P = 0.0002$) in a dose-dependent manner (Fig. 8C). Combinations that contained the lowest dose of gentamicin (1.25 mg/kg) generally fared poorly (Fig. 8D). However, addition of Octa-C10 at 10 mg/kg ($P = 0.0067$), 5 mg/kg ($P = 0.0031$), or 2.5 mg/kg ($P = 0.0093$), a dose that has no effect when applied alone, increased survival relative to 1.25 mg/kg gentamicin alone, where survival was worst (Fig. 8A and D), and the combination with 5 mg/kg Octa-C10 offered modest but significant protection, rescuing 36% ($P = 0.0403$). Therefore, the *in vivo* outcomes from attempted burn wound infection therapy indicate that combining gentamicin and Octa-C10 leads to either modest synergy or, at worst at suboptimal doses, an additive effect.

DISCUSSION

The present SAR study of bolalipids based on CM2 shows that increasing head-group bulk and/or reducing overall hydrophobicity reduces plasmid intercalation and/or topoisomerase I inhibition, effects expected to mitigate the risk of genotoxicity (16).

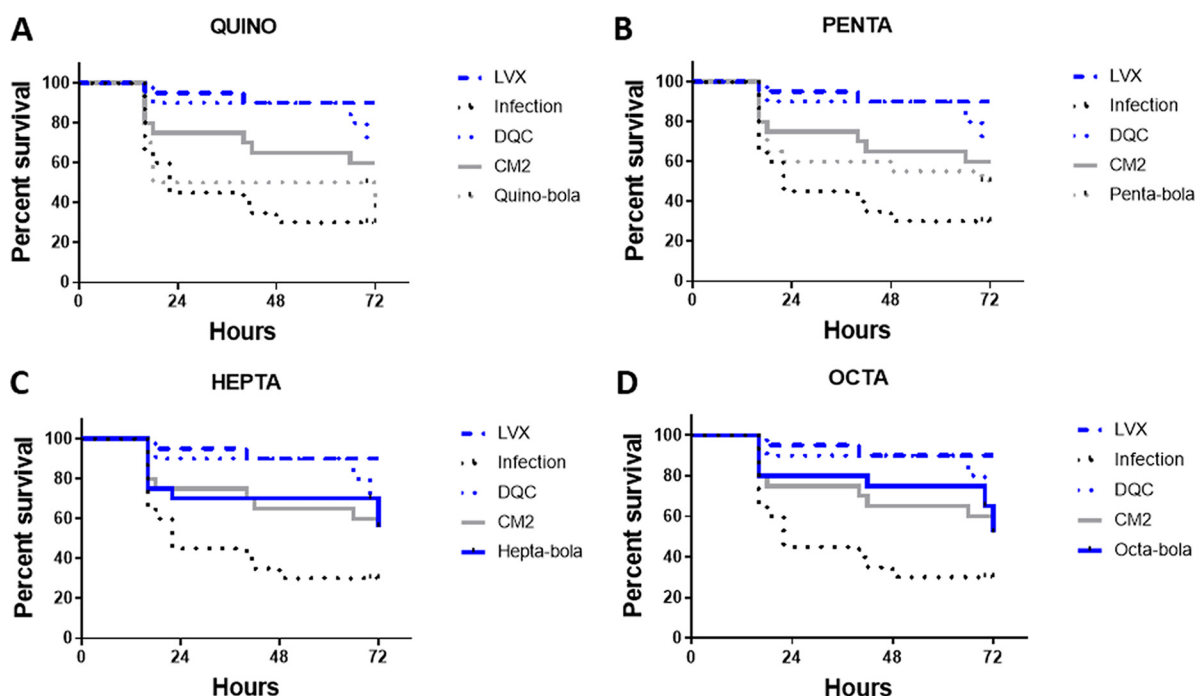


FIG 7 Bolalipids are protective in a *G. mellonella* model of *E. coli* ATCC 25922 infection. Survival curves over 72 h are plotted for 20 larvae, each treated with a single 10-mg/kg dose of Quino-bola (A), Penta-bola (B), Hepta-bola (C), or Octa-bola (D), in each case compared with 10 mg/kg CM2 or DQC or 2 mg/kg levofloxacin (LVX). Blue curves indicate significant protection according to a log rank (Mantel-Cox) test (CM2 $P = 0.0527$).

These modifications also reduced antimicrobial activity against *Candida* spp. In contrast, while reducing the overall hydrophobicity similarly mitigated cytotoxicity and reduced antibacterial potency, increasing the headgroup size had the opposite effect.

Synergy between bolalipids and antibiotics relevant to clinical or veterinary settings was observed. A substantial increase in the *P. aeruginosa* killing rate was observed when only a small amount of bolalipid was used in combination with tobramycin, which is otherwise weakly bactericidal. However, while synergy was strong for any bolalipid combination with either gentamicin or tobramycin against *A. baumannii* or *P. aeruginosa*, no synergy was observed for other Gram-negative bacteria, and it was weaker for another aminoglycoside, streptomycin, against *Ac. pleuropneumoniae*.

The *in vitro* selectivity indices suggested that shorter acyl linker chain bolalipids had the greatest potential for treatment of mycobacteria infections. However, therapy of *M. tuberculosis* Bleupan infection was achieved only with a bolalipid with a longer acyl linker, while the more soluble analogue, with a shorter acyl linker, exacerbated the infection. Longer acyl linker analogues also offered some protection against *E. coli* ATCC 25922 despite comparatively poor *in vitro* selectivity indices for Gram-negative bacteria. These findings suggest that the power of *in vitro* assays to predict therapeutic success may be limited for this class of antimicrobial.

We therefore considered the implications of these findings for our understanding of the mechanisms of the bolalipid antimicrobial activity against diverse pathogens and whether and how the bolalipids might be further developed toward use in a broader range of indications.

Mechanisms of toxicity and antimicrobial activity. Bolalipid antimicrobials, for which the lead of the class is DQC, have a wide variety of effects on different cell components, and there is no single well-defined target. The mitochondrial toxicity of DQC, which is associated with mitochondrial swelling and inhibition of the mitochondrial respiratory chain, is due to lipophilicity and to its delocalized positive charge, characteristics that enable the molecule to readily penetrate the lipid bilayers of mitochondria (7). DQC also induces selective depletion of mitochondrial DNA in human cells (17) and

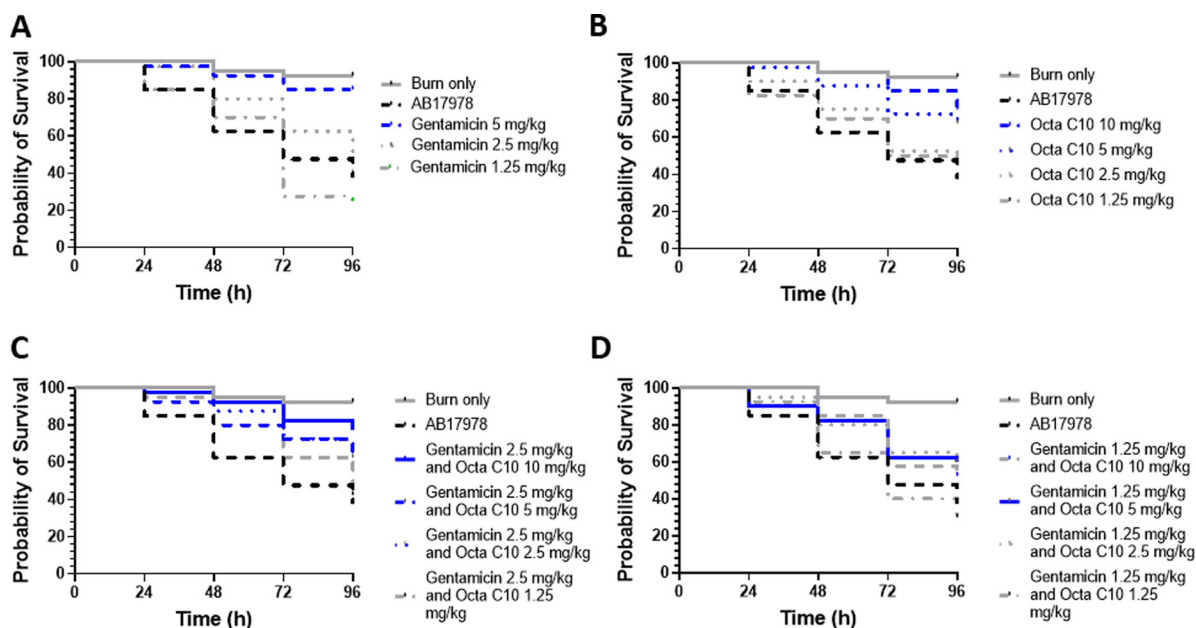


FIG 8 New bolalipids are protective alone or in combination with gentamicin in a *G. mellonella* model of *A. baumannii* ATCC 17978 burn wound infection. Survival curves were plotted for 40 larvae, each treated with various doses of gentamicin (A) or Octa-C10 (B) or with 2.5 mg/kg (C) or 1.25 mg/kg (D) gentamicin plus various doses of Octa-C10. Results in each case were compared with burn only or burn plus infection (*A. baumannii* 17978) over 96 h. Blue curves indicate significant protection ($P < 0.05$) against infection, due to therapy, according to a log rank (Mantel-Cox) test (burn-only $P < 0.0001$).

breaks down mitochondrial DNA in the yeast *Saccharomyces cerevisiae*, which induces the formation of petite (respiration-deficient) mutants (18). As such, bolalipids may have acute toxic effects on mitochondria and mammalian cells but may also cause delayed-onset effects that nevertheless inhibit both mammalian and fungal cell growth. Consistent with this, since the overall lipophilicity is similar and the delocalized positive charge is retained, none of the headgroup modifications presented here substantially affect cytotoxicity. The present SAR study is also consistent with an important role for DNA binding in inhibiting fungal growth. While all bolalipids retain antifungal activity, likely due to the acute impact on mitochondrial respiration, bolalipids with larger headgroups, which are less able to intercalate in DNA, are also less effective inhibitors of *Candida* spp.

DQC is also rapidly taken up by bacterial cells, penetrating rapidly into the cytoplasm, but its capacity for damaging the plasma membrane is low (19). On entering the bacterial cell, DQC is liable to precipitate cytoplasmic material, most notably nucleic acid, while dehydrogenase activity is also inhibited, potentially impacting respiration (19). In contrast with the antifungal SAR described above, the extent to which nucleic acid precipitation contributes to bolalipid bactericidal activity is unclear, even if this is unrelated to DNA intercalation, since some bolalipids that have the lowest DNA intercalation potential are nevertheless potent antibacterial compounds. Indeed, unlike the results presented above, where bolalipids with larger headgroups were less effective against *Candida* spp., bolalipids with larger headgroups are more potent against both Gram-positive and Gram-negative bacteria *in vitro* and are protective against *E. coli* infection *in vivo*. This finding is consistent with previous work that showed that delocalized positive charge, larger headgroup, and longer chain are important features for the antimicrobial activity of quaternary ammonium surfactants (20). This study also identified three modes of antibacterial action in the series of quaternary ammonium surfactants. At low concentrations, bacterial energetics and cell division were impaired. At intermediate concentrations membrane permeabilization and inhibition of electron transport was observed. Disruption of bacterial membranes and cell lysis occurred only at concentrations close to the critical micellar concentration. Given the relatively high potency of the bolalipids described here, the structural modifications that

impact antibacterial potency may therefore modulate bolalipid impact on bacterial energetics and/or cell division.

Mechanism of bolalipid-aminoglycoside synergy. The ability of the cationic bolalipids to accumulate in cells may also underpin their ability to act in strong synergy with the aminoglycosides tobramycin and gentamicin against *P. aeruginosa* (and *A. baumannii*). Tobramycin is positively charged at physiological pH and interacts electrostatically with bacterial membranes but requires entry to the bacterial cytosol to exert its main mechanism of action, which consists of inhibiting bacterial protein synthesis by preventing the formation of the complex between the bacterial 70S ribosome and mRNA. Being a very hydrophilic molecule, however, it cannot passively cross the membrane and instead exploits the proton motive force to enter the cell (21).

An antimicrobial that acts in synergy with tobramycin might therefore be expected to facilitate its transfer to ribosomes after crossing the cytoplasmic membrane, interfere with aminoglycoside-modifying enzymes, or simply increase its intracellular concentration. It appears unlikely that the latter is achieved by bolalipids damaging the cell wall and hence increasing permeability, since their potential to disrupt bilayer integrity was shown here to be low. Further, the same potentiation of tobramycin was obtained even with bolalipids (e.g., Octa-C6) that are relatively inactive against bacteria when used alone, and much weaker or no synergy was observed between bolalipids and either tobramycin or gentamicin against other Gram-negative bacteria. Instead, it is possible that further investigation of the phenomenon will reveal that increased tobramycin intracellular accumulation is achieved by stimulating its uptake. This has been observed for amphiphilic rhamnolipids, produced by *P. aeruginosa*, which facilitate proton motive force-independent tobramycin uptake in *Staphylococcus aureus*, and fumarate, which increases cellular respiration and proton motive force (22, 23). If the synergistic combination of bolalipids and tobramycin relies on bolalipids increasing *P. aeruginosa* cellular respiration, then the infection setting may strongly influence whether this is possible and the scope for the future development of such combinations in differing indications. Nevertheless, as recently achieved by others using photodynamic therapy (24) or light-activated molecular machines (25), successful therapy of *A. baumannii*-infected burn wounds in *G. mellonella*, with Octa-C10 both alone and in combination with gentamicin, suggests that further evaluation in mammalian infection models may be warranted. While gentamicin sulfate cream is widely used to treat burn wound infections, aminoglycoside resistance in *P. aeruginosa* and *A. baumannii* is an acute problem (26, 27). Future research may uncover whether bolalipids can be used to counter aminoglycoside resistance in burn wounds and, due to the rapid bactericidal activity, treat infections more rapidly.

Factors that will influence further development. None of the bolalipid headgroup or acyl linker modifications substantially affect antimicrobial activity against mycobacteria. As such, a promising *in vitro* selectivity index for *M. tuberculosis* Bleupan activity over toxicity was obtained for Octa-C6, a bolalipid that also has weak intercalation/topoisomerase I inhibition potential. However, rather than offering protection against infection in *G. mellonella*, at relatively low doses Octa-C6 exacerbated the infection. Octa-bola, which was similarly potent *in vitro* but which had a much poorer selectivity index, was paradoxically much better tolerated *in vivo* and offered protection at intermediate doses. It was also notable that DQC also exacerbated *M. tuberculosis* Bleupan infection in *G. mellonella*. DQC was substantially less potent than Octa-bola against *M. tuberculosis* Bleupan *in vitro* but was nevertheless more potent against this pathogen than it was against *E. coli*, against which DQC offered some protection *in vivo*. A better understanding of the relationships between *in vitro* activities and *in vivo* therapeutic performance may require investigation of how different classes of antimicrobials interact with, and different pathogens respond to, the innate immune system. Notably, antimicrobials that are mitochondrial poisons will likely impair the oxidative burst of hemocytes. However, the relative *in vivo* performance against *M. tuberculosis* Bleupan does suggest a pathway for future development. CM2 was designed to have better self-assembly properties than DQC, with acyl linker length and bulkiness of the headgroup aliphatic residue being important determinants, and the headgroup of Octa-bola is bulkier still. As expected, Octa-bola had the greatest ability to form nanoparticles and Octa-C6 the least, reflecting substantially different tendencies of these bolalipids to

form aggregates. These data are insufficient to provide a mechanistic explanation but suggest future avenues to improve understanding of determinants of *in vivo* outcomes. We speculate that self-assembly, or effects related to this property, may have a critical impact on parameters such as biodistribution and local versus generalized impacts on the host innate immune system. Therefore, in spite of poor *in vitro* toxicity profiles, better self-assembly properties may be critical in determining *in vivo* therapeutic outcomes, and bolalipids with this property may offer a better foundation for future development.

Conclusion. Taken together, the results of the SAR approach used in the present study provide a better understanding of the differing mechanisms that underpin bolalipid antimicrobial activity against Gram-positive and Gram-negative bacteria, *Candida* spp., and mycobacteria. Further, while the genotoxicity of the bolalipids may be mitigated by structural modification, cytotoxicity is unaffected and remains a substantial hurdle to repurposing bolalipids for a wider range of microbial indications. Nevertheless, the discovery of bolalipid synergy with aminoglycosides and resensitization of aminoglycoside-resistant strains of *P. aeruginosa* and *A. baumannii*, coupled with the observation of successful therapy in four of five *G. mellonella* infection models with bolalipids with longer acyl linkers, suggests that formulations that can serve to mitigate the availability of soluble bolalipid before reaching the microbial target may unlock wider utility of this group of antimicrobial lipids, even if it is initially limited to topical application.

MATERIALS AND METHODS

Synthesis. The designed compounds (Fig. 1) were synthesized via solution chemistry techniques. Purification procedures involved flash chromatography, liquid-liquid extraction, high-pressure liquid chromatography (HPLC), and ion exchange. All the intermediates and the final products were characterized by ^1H and ^{13}C nuclear magnetic resonance (NMR), low-resolution mass spectrometry (LRMS), and high-resolution MS (HRMS) techniques to verify and confirm the formation of the desired compounds. Details about the synthesis and purification processes can be found in the supplemental material.

Unwinding assay. A DNA unwinding assay kit (Inspiralis Limited, Norwich, UK) consists of wheat germ topoisomerase I assay buffer (50 mM Tris HCl [pH 7.9], 1 mM EDTA, 1 mM dithiothreitol [DTT], 20% [vol/vol] glycerol, 50 mM NaCl) dilution buffer (50 mM Tris HCl [pH 7.9], 1 mM EDTA, 1 mM DTT, 50% [vol/vol] glycerol, 500 mM NaCl), wheat germ topoisomerase I (5 U/ μL), supercoiled plasmid pBR322 (1 $\mu\text{g}/\mu\text{L}$), and relaxed plasmid pBR322 (1 $\mu\text{g}/\mu\text{L}$). For the experiments, 2 \times DNA loading buffer containing 40% (wt/vol) sucrose, 100 mM Tris-HCl (pH 8), 1 mM EDTA, and 0.5 mg/mL bromophenol blue was prepared. The enzyme was diluted 1/5 with dilution buffer before being used in the assay. For the assay, 3 mM stock solutions in methanol of the compounds to be tested were prepared. An appropriate number of 1.5-mL Eppendorf tubes were filled with 25 μL of a mix consisting of assay buffer (15 μL of buffer per sample), supercoiled or relaxed pBR322 (0.5 $\mu\text{g}/\text{assay}$), and ultrapure water. In the first two tubes, 1 μL of methanol was added to test the effect of the solvent on both the plasmid and the enzyme. Subsequently, 1 μL of the test compounds was added to the remaining tubes, and the tubes briefly vortexed and incubated at room temperature for 5 min. After that, 2 μL of dilution buffer was added in the first tube, whereas 2 μL of enzyme diluted solution was added to the remaining tubes. The tubes were gently vortexed and incubated for 30 min at 37°C in a water bath. After this time, the reaction was stopped by adding 20 μL of water and 50 μL of water-saturated butanol to each tube. The tubes were vortexed and centrifuged for 1 min at 14,800 rpm. The lower aqueous layer of each tube was removed and transferred to a new tube containing 30 μL of chloroform-isoamyl alcohol (24/1) and 50 μL of loading buffer. The tubes were briefly vortexed and centrifuged for 1 min. Twenty microliters of the upper layer of each tube was loaded onto a 1% (wt/vol) agarose gel, and the gel was run at 80 V for approximately 4 h in Tris-acetate-EDTA buffer (40 mM Tris acetate and 1 mM EDTA). Subsequently, the gel was stained with ethidium bromide (1 $\mu\text{g}/\text{mL}$) for 15 min, briefly destained (5 to 10 min) in water, and visualized with a Multi-Doc Imaging M-26X UVP transilluminator.

Antibacterial activity assay. The antibacterial activity of the bolalipids was assessed through a modified 2-fold broth microdilution assay with modal MICs generated from at least three biological replicate experiments (28). The method broadly followed EUCAST methodology, with non-cation-adjusted Mueller-Hinton broth replacing cation-adjusted Mueller-Hinton broth for panels of Gram-negative bacteria, Gram-positive bacteria, and fungi (Tables 1 to 3), Middlebrook 7H9 broth (Difco, Detroit, MI, USA) supplemented with 10% (vol/vol) oleic acid-albumin-dextrose-catalase (OADC) enrichment (Becton, Dickinson, Franklin Lakes, NJ, USA) and 0.5% (vol/vol) glycerol for *Mycobacterium smegmatis* mc² 155 and *M. tuberculosis* Bleupan (Tables 1 to 3), brain heart infusion (BHI) broth with 5% horse serum for *Gardnerella vaginalis* and *Prevotella bivia* (Table 4), and BHI with 5% fetal bovine serum (FBS) and 0.01% NAD for *Actinobacillus pleuropneumoniae* and *Glaesserella parasuis* (Table 5). *G. vaginalis* and *P. bivia* MIC testing was conducted under anaerobic conditions generated using Thermo Scientific Oxoid AnaeroGen. Bolalipids and antibiotics were diluted in a 2-fold dilution in media down a sterile, polypropylene 96-well plate (Greiner Bio-One GmbH, Frickenhausen, Germany). Bacteria were then added, back-diluted from an overnight culture, at a starting concentration of 5×10^5 CFU/mL. Plates were incubated statically at 37°C for 20 h, and the optical density at 600 nm (OD₆₀₀) was determined using a Clariostar plate reader (BMG

Labtech). The MIC was defined as the lowest concentration where growth was <0.1 above the background absorbance. Synergy was measured using either a fixed concentration of bolalipid ($0.25 \times$ MIC) combined with doubling dilutions of antibiotic, or standard microdilution checkerboard assays under the same conditions as the MICs (29). For the fixed-concentration assays, 2-fold dilution series of the antibiotics were prepared, and then bolalipid was added at a final concentration of $0.25 \times$ MIC, followed by addition of bacteria. The MIC of the antibiotic in combination with bolalipid was defined as above. For the checkerboard assays, 2-fold dilution series of each antibiotic were prepared in separate 96-well plates and then combined into one before addition of bacteria. The growth/no-growth interface was determined using the same definition as the MIC. The fractional inhibitory concentration (FIC) was calculated from the most synergistic well on the plate for three independent repeats, and values are presented as averages and standard deviations. The FIC is calculated as (MIC of compound A in combination with B/MIC of compound A alone) + (MIC of compound B in combination with A/MIC of compound B alone). MICs were determined on the same plates as the FICs to increase reproducibility. FIC values of ≤ 0.5 were considered to indicate strong synergism and, consistent with a recent re-evaluation of FIC, which stressed the importance of also measuring the MIC in the same microarray plate, values of 0.5 to <1 were considered to indicate weak synergism (29).

Dynamic light scattering. Stock solutions of bolalipids were prepared by dispersing the powder in ultrapure water, then stirring vigorously by vortexing, and sonicating in a 40°C bath sonicator for 20 min. The concentration of each stock solution corresponds to the highest solubility achieved in water for each bolalipid, using the method described above. DLS experiments were performed on a Malvern Zetasizer Nano (Malvern Instruments, Worcestershire, UK) in back-scattering mode at 20°C . There were three independent measurements of each sample and 12 runs for each measurement, with 10 s taken for each run. The attenuator index and measurement position were automatically adjusted. Fifty microliters of each sample was transferred into polystyrene semi-microcuvettes for determination of UV and visible wavelengths (Sarstedt).

Electrophysiology (patch-clamp) experiments. Giant unilamellar vesicles (GUVs) composed of DiPhytanoly PhosphatidylGlycerol (DPhPG) were prepared in the presence of 1 M sorbitol by the electroformation method in an indium-tin oxide (ITO)-coated glass chamber connected to the Nanion Vesicle Prep Pro setup (Nanion Technologies GmbH, Munich, Germany) using a 3-V peak-to-peak AC voltage at a frequency of 5 Hz for 140 min at 37°C (30–32). Bilayers were formed by adding the GUV solution to a buffer containing 250 mM KCl, 50 mM MgCl_2 , and 10 mM HEPES (pH 7.00) onto an aperture in a borosilicate chip (Port-a-Patch; Nanion Technologies) and applying 7,000 to 9,000 Pa negative pressure, resulting in a solvent-free membrane with a resistance in the $\text{G}\Omega$ range. Diphytanoyl chains were used here for practical reasons, since, unlike lipids with mixed palmitoyl-oleoyl chains, these lipids do not undergo the main, temperature-dependent transition from disordered fluid into the all-*trans* configuration and remain in the same phase between -120° and $+120^\circ\text{C}$ (33) while, crucially, the membranes composed of these lipids are mechanically stable and have high specific resistance (34), essential for electrophysiology experiments. After formation, a small amount of bolalipid stock solution (in water) was added to 50 μL of buffer solution in order to obtain its active concentration. All the experiments were carried out with a positive holding potential of 50 mV. The active concentration, the concentration at which the bolalipid first showed membrane activity, for each bolalipid was obtained through a titration performed under the same conditions. For all the experiments, a minimum of 6 concordant repeats were done. Current traces were recorded at a sampling rate of 50 kHz using an EPC-10 amplifier from HEKA Elektronik (Lambrecht, Germany). The system was computer controlled by PatchControl software (Nanion) and GePulse (Michael Pusch, Genoa, Italy [<http://users.ge.ibf.cnr.it/pusch/software-mik.html>]). The data were filtered using the built-in Bessel filter of the EPC-10 amplifier at a cutoff frequency of 10 kHz. The experiments were performed at room temperature. Data analysis was performed with the pClamp 10 software package (Axon Instruments).

Fluorescence spectroscopy. Bolalipid fluorescence spectra were recorded in water; 0.45 mM and 0.18 mM solutions of CM2 and DQC were prepared by dispersing the powder in ultrapure water, then stirring vigorously by vortexing, and sonicating in a bath sonicator at 40°C . A Varian Cary Eclipse spectrophotometer was used to record fluorescence intensity. Seven hundred microliters of each bolalipid solution was transferred into a Hellma Analytics UV quartz cuvette with a light path of 10 mm and used for each recording. For both bolalipids, the excitation wavelength was set to 350 nm while the emission range was from 352 nm to 600 nm, and the averages for 20 scans were obtained.

Fluorescence microscopy. *P. aeruginosa* PAO1 was incubated with CM2 alone or in combination with tobramycin. A single colony of bacteria was collected from a Luria-Bertani (LB) agar plate and resuspended in 10 mL of LB broth overnight at 37°C , with shaking at 150 rpm. The following morning, a 2% (vol/vol) dilution was done in fresh LB broth, and the bacteria suspension was grown at 37°C with shaking at 150 rpm until it reached an OD_{600} of 0.3. The surface of microscopy SuperFrost glass slides (Thermo Fisher Scientific, Massachusetts, USA) was marked with a PAP pen, in order to design two square confined areas per glass slide, where the bacteria were deposited. One hundred microliters of bacterial suspension was transferred into sterile Eppendorf tubes and incubated with equal volumes of bolalipid suspension for 1 h. The bolalipid final concentration was 0.18 mM. The fluorescent Alexa Fluor 555 conjugate of wheat germ agglutinin (WGA) (Thermo Fisher Scientific) lectin membrane dye (10 $\mu\text{g}/\text{mL}$ final concentration) was added to the suspension, and the bacteria were incubated for 45 min more. At the end of incubation, 100 μL was spotted in each half of the SuperFrost glass slides and incubated for 45 min more. Glass slides were then washed three times with phosphate-buffered saline (PBS) and left to dry for 5 min before addition of one drop of Fluoromount (Sigma-Aldrich, Germany) aqueous mounting medium. Confocal images were acquired with a Zeiss LSM800

microscope (Zeiss, Germany) and elaborated with ZEN software. Excitation and emission filter wavelengths were, respectively, 352 nm and 455 nm for CM2 and 541 nm and 565 nm for WGA555.

Candida auris cells were picked from a yeast extract-peptone-dextrose (YPD) agar plate and resuspended in 35 mL of sterile distilled water (dH₂O). After resuspension, 150 μ L of cells was inoculated in 100 mL of YPD broth overnight at 30°C with shaking at 130 rpm and grown to exponential phase (5×10^6 to 5×10^7 cells/mL). Cells (6×10^8) were washed in standard defined (SD) medium twice (pelleted at $1,500 \times g$ for 5 min and resuspended in 10 mL SD medium [yeast nitrogen base without the amino acids D-glucose, methionine, adenine, histidine, tryptophan, uracil, leucine, and lysine]), followed by resuspension in 1 mL SD medium containing 0.18 mM Penta-bola, and incubated at 37°C for 30 min. After treatment with the Penta-bola, cells were pelleted and resuspended in Hanks' balanced salt solution (HBSS) and 50 μ g/mL CF594 concanavalin A (Biotium). After incubation at 37°C for 30 min, cells were washed once with HBSS and resuspended in 1 mL of HBSS. Polysine adhesion slides (Thermo Scientific) were prepared by spreading 20 μ L of treated cells and allowing them to dry for 30 min before adding one drop of Fluoromount (Sigma-Aldrich, Germany) aqueous mounting medium. Fluorescence images were acquired using a Leica fluorescence microscope at $\times 100$ magnification. Excitation and emission filter wavelengths were 358 nm and 461 nm for Penta-bola and 593 nm and 614 nm for CF594 concanavalin A, respectively.

In vitro PD assays were performed with *Pseudomonas aeruginosa* RP73 cultured in Roswell Park Memorial Institute 1640 medium (RPMI) supplemented with 5% Mueller-Hinton broth (MHB) (35). Bacteria were cultured overnight in 10 mL of RPMI-5% MHB at 37°C and diluted just prior to plate inoculation to an OD₆₀₀ of 0.002. Stock solutions of colistin or tobramycin were prepared in sterile MilliQ water at a concentration of 200 \times MIC. Octa-bola was prepared in methanol at 2,000 \times MIC and diluted in water to 200 \times MIC. A dilution series was made in the top row of a polypropylene 96-well plate from 200 \times MIC to 0.2 \times MIC in a volume of 100 μ L, to which 100 μ L of the bacterial suspension was added to have a total of 1×10^6 log-phase CFU in 200 μ L. The first time zero sample was taken <30 s after addition of bacteria to the plate, with further samples taken at appropriate intervals thereafter. Octa-bola-tobramycin-challenged bacteria were sampled every 20 min for 120 min due to rapid killing, while tobramycin- and colistin-challenged bacteria were sampled every hour for 6 h. Fifteen microliters was removed from each well, diluted 1:1,000 in phosphate-buffered saline, and plated onto RPMI-5% MH agar plates. The plates were incubated at 37°C overnight for CFU counting.

CFU data were log₁₀ transformed, and the bacterial net growth rate was determined from the increase or decrease in CFU during the time of exposure to the antibiotics as the coefficient of a linear regression of log₁₀ CFU as a function of time. The intercept of the regression was fixed by forcing the regression lines through the first CFU measurement (0 min) at a given antimicrobial concentration. The pharmacodynamic function according to Regoes et al. (36) describes the relationship between bacterial net growth rate (ψ) and the concentration of an antimicrobial (a): $\psi_{\max} - ([\psi_{\max} - \psi_{\min}][a/zMIC])^{\kappa} / ([a/zMIC]^{\kappa} - [\psi_{\min}/\psi_{\max}])$. Fitting this function to the net bacterial growth rates in OriginPro 2020 (OriginLab Corporation, Northampton, MA) generates the parameters ψ_{\min} and ψ_{\max} (minimum and maximum growth rates, respectively), zMIC (the pharmacodynamic MIC), and κ (a measure of the cooperativity). Average parameters obtained from fits of three or more independently repeated experiments were compared by one-way analysis of variance (ANOVA) with Tukey's *post hoc* test. Since the CFU data are log₁₀ transformed, the net growth rates are reported to three significant figures.

Galleria mellonella infection models. The antimicrobial activities of DQC, CM2, and its analogues Quino-bola, Penta-bola, Hepta-bola, and Octa-bola against *Escherichia coli* ATCC 25922 were tested in *Galleria mellonella* larvae. All assays were performed on two separate occasions using a group size of 10 larvae; the larvae were kept in separate petri dishes and in a static incubator at 37°C during the period of the experiment. A suspension of *E. coli* ATCC 25922 was prepared by transferring two colonies of *E. coli* ATCC 25922 from a fresh agar plate into PBS and adjusting the absorbance to a McFarland 0.5 standard. The number of CFU per milliliter of this suspension was determined and corresponded to 1×10^8 CFU/mL. Larvae were injected beneath the tegument with 10 μ L of a 1×10^7 -CFU/mL bacteria suspension, corresponding to 1×10^5 CFU per larva. A 50- μ L Hamilton syringe with a G27 needle was used for the injection. Stock solutions of bolalipid analogues were prepared at a concentration of 250 μ g/mL with DQC at 200 μ g/mL due to its poor solubility. Ten microliters of stock solution was injected into each larva 1 h after infection (10 mg/kg). Levofloxacin (LVX; 50 μ g/mL = 2 mg/kg) and PBS were used as positive and negative controls, respectively. A noninfected PBS injection was included to control for the effects of injection. Survival was monitored over a period of 70 to 72 h. Changes in *G. mellonella* survival were analyzed by the log rank (Mantel-Cox) method and plotted as Kaplan-Meier survival curves using GraphPad Prism version 7.

The procedure was similar for EMRSA-15, *P. aeruginosa* RP73, and *M. tuberculosis* Bleupan infections with the following modifications. For EMRSA-15, larvae were injected with 10 μ L of a 1×10^7 CFU/mL suspension with treatment by single injection initiated 2 h postinfection. Survival was monitored for 144 h postinfection. For *P. aeruginosa* RP73, overnight cultures were prepared from a single colony, and following dilution in PBS, larvae were injected with 10 μ L of either a 1×10^6 -CFU/mL or 1×10^3 -CFU/mL bacterial suspension, corresponding to 1×10^2 CFU or 1×10^1 CFU per larva. Treatment was a single injection, 2 h after infection, with 5 or 50 mg/kg vancomycin as controls. Survival was monitored over a period of 96 h.

For *M. tuberculosis* Bleupan, a mid-log-phase culture was prepared from a glycerol stock and washed and diluted in PBS containing 0.05% polysorbate-80 (PBS-T) to produce a bacterial suspension of 2×10^9 CFU/mL. Of this, 10 μ L was injected, corresponding to 2×10^7 CFU per larva. Treatment was given as a single injection, 1 h postinfection. Larval survival was monitored over 96 h. For positive and

negative controls, rifampin (RIF; 200 $\mu\text{g}/\text{mL}$ = 10 mg/kg) and PBS-T were used, respectively. A noninfected control using PBS-T was used as described above.

In addition to the intrahemocoelic infection/therapy models described above, a recently described *G. mellonella* burn wound model was adopted (37). The burn was created using the flat head of a nail, which was heated in a blue Bunsen burner flame until red hot, cooled for 15 s, and superficially applied for 2 s to generate a 2-mm² burn. Larvae were then infected with a single colony of *A. baumannii* ATCC 17978 applied directly to the burn site, or sterile phosphate-buffered saline was applied as a control. Treatment was applied topically 1 h after infection in a volume of 5 μL . Survival was monitored over 96 h.

SUPPLEMENTAL MATERIAL

Supplemental material is available online only.

FIG S1, PDF file, 0.1 MB.

FIG S2, PDF file, 0.3 MB.

FIG S3, PDF file, 0.01 MB.

TABLE S1, PDF file, 0.1 MB.

TABLE S2, PDF file, 0.1 MB.

TABLE S3, PDF file, 0.1 MB.

ACKNOWLEDGMENTS

This work was supported by a BBSRC CASE studentship (BB/L013576/1) for S.D.B. awarded to A.J.M., an NC3Rs Skills & Knowledge Transfer grant (NC/T001240/1), a joint HKU-KCI studentship for D.K.-W.M. awarded to J.K.W.L., Public Health England, and Procarta Biosystems Ltd. and by the King's Together Multi and Interdisciplinary Research Scheme (Wellcome Trust Institutional Strategic Support Fund; grant reference [204823/Z/16/Z]).

A.J.M. and S.D.B. wrote the main manuscript text and prepared all figures. S.D.B., M.M., and A.J.M. designed the overall experimental approach. S.D.B. together with M.M. and A.J.M. designed the 12-bis-THA Cl₂ analogues, which were synthesized and purified by S.D.B. with A.B. and C.A. S.D.B., C.K.H., M.C., V.H., J.B., Y.L., P.R.L., and J.M.S. designed and/or conducted MIC and/or FIC testing. M.C., G.M., and S.V.D.L. designed and conducted *in vitro* pharmacodynamic assays. S.D.B., M.C., M.A., D.S., L.L., C.L., and E.G. conducted *in vivo* testing in *Galleria mellonella*. D.K.-W.M., J.K.W.L., and B.D.R. designed and/or conducted *in vitro* assays with *M. smegmatis* and *M. tuberculosis* Bleupan. S.D.B. and L.L. performed confocal studies with *P. aeruginosa*, and M.H. and B.P. performed confocal studies with *C. auris*. All authors approved the manuscript.

We declare no competing financial interest.

REFERENCES

- O'Neill J. 2016. Tackling drug-resistant infections globally: final report and recommendations. https://amr-review.org/sites/default/files/160518_Final%20paper_with%20cover.pdf. Accessed 18 May 2017.
- Antimicrobial Resistance Collaborators. 2022. Global burden of bacterial antimicrobial resistance in 2019: a systematic analysis. *Lancet* 399:629–655. [https://doi.org/10.1016/S0140-6736\(21\)02724-0](https://doi.org/10.1016/S0140-6736(21)02724-0).
- Fuhrhop J-H, Wang Y. 2004. Bolaamphiphiles. *Chem Rev* 104:2901–2937. <https://doi.org/10.1021/cr030602b>.
- Mendling W, Weissenbacher ER, Gerber S, Prasauskas V, Grob P. 2016. Use of locally delivered dequalinium chloride in the treatment of vaginal infections: a review. *Arch Gynecol Obstet* 293:469–484. <https://doi.org/10.1007/s00404-015-3914-8>.
- Gamboa-Vujicic G, Emma DA, Liao SY, Fuchtnet C, Manetta A. 1993. Toxicity of the mitochondrial poison dequalinium chloride in a murine model system. *J Pharm Sci* 82:231–235. <https://doi.org/10.1002/jps.2600820302>.
- Tischer M, Pradel G, Ohlens K, Holzgrabe U. 2012. Quaternary ammonium salts and their antimicrobial potential: targets or nonspecific interactions? *ChemMedChem* 7:22–31. <https://doi.org/10.1002/cmdc.201100404>.
- Belosludtsev KN, Belosludtseva NV, Tenkov KS, Sharapov VA, Kosareva EA, Dubinin MV. 2018. Effect of dequalinium on respiration and the inner membrane permeability of rat liver mitochondria. *Biochem Moscow Suppl Ser A* 12:121–127. <https://doi.org/10.1134/S1990747818020034>.
- Weissig V, Lizano C, Ganellin C, Torchilin V. 2001. DNA binding cationic bolosomes with delocalized charge center. A structure-activity relationship study. *STP Pharma Sci* 11:91–96.
- Mamusa M, Resta C, Barbero F, Carta D, Codoni D, Hatzixanthos K, McArthur M, Berti D. 2016. Interaction between a cationic bolaamphiphile and DNA: the route towards nanovectors for oligonucleotide antimicrobials. *Colloids Surf B Biointerfaces* 143:139–147. <https://doi.org/10.1016/j.colsurfb.2016.03.031>.
- Mansouri A, Haouzi D, Descatoire V, Demeilliers C, Sutton A, Vadrot N, Fromenty B, Feldmann G, Pessayre D, Berson A. 2003. Tacrine inhibits topoisomerases and DNA synthesis to cause mitochondrial DNA depletion and apoptosis in mouse liver. *Hepatology* 38:715–725. <https://doi.org/10.1053/jhep.2003.50353>.
- Ng CKL, Singhal V, Widmer F, Wright LC, Sorrell TC, Jolliffe KA. 2007. Synthesis, antifungal and haemolytic activity of a series of bis(pyridinium)alkanes. *Bioorg Med Chem* 15:3422–3429. <https://doi.org/10.1016/j.bmc.2007.03.018>.
- Laborda P, Alcalde-Rico M, Blanco P, Martinez JL, Hernando-Amado S. 2019. Novel inducers of the expression of multidrug efflux pumps that trigger *Pseudomonas aeruginosa* transient antibiotic resistance. *Antimicrob Agents Chemother* 63:e01095-19. <https://doi.org/10.1128/AAC.01095-19>.
- Manzo G, Ferguson PM, Gustilo VB, Hind C, Clifford M, Bui TT, Drake AF, Atkinson RA, Sutton MJ, Batoni G, Lorenz CD, Phoenix DA, Mason AJ. 2019. Minor sequence modifications in temporin B cause drastic changes in antibacterial potency and selectivity by fundamentally altering membrane activity. *Sci Rep* 9:1385. <https://doi.org/10.1038/s41598-018-37630-3>.
- Manzo G, Ferguson PM, Hind C, Clifford M, Gustilo VB, Ali H, Bansal SS, Bui TT, Drake AF, Atkinson RA, Sutton JM, Lorenz CD, Phoenix DA, Mason AJ. 2019. Temporin L and aurein 2.5 have identical conformations but subtly

- distinct membrane and antibacterial activities. *Sci Rep* 9:10934. <https://doi.org/10.1038/s41598-019-47327-w>.
15. Manzo G, Hind CK, Ferguson PM, Amison RT, Hodgson-Casson AC, Ciazynska KA, Weller BJ, Clarke M, Lam C, Man RCH, Shaughnessy BGO, Clifford M, Bui TT, Drake AF, Atkinson RA, Lam JKW, Pitchford SC, Page CP, Phoenix DA, Lorenz CD, Sutton JM, Mason AJ. 2020. A pleurocidin analogue with greater conformational flexibility, enhanced antimicrobial potency and in vivo therapeutic efficacy. *Commun Biol* 3:697. <https://doi.org/10.1038/s42003-020-01420-3>.
 16. Ferguson LR, Denny WA. 2007. Genotoxicity of non-covalent interactions: DNA intercalators. *Mutat Res* 623:14–23. <https://doi.org/10.1016/j.mrfmmm.2007.03.014>.
 17. Schneider-Berlin KR, Ammini CV, Rowe TC. 1998. Dequalinium induces a selective depletion of mitochondrial DNA from HeLa human cervical carcinoma cells. *Exp Cell Res* 245:137–145. <https://doi.org/10.1006/excr.1998.4236>.
 18. Schneider-Berlin KR, Bonilla TD, Rowe TC. 2005. Induction of petite mutants in yeast *Saccharomyces cerevisiae* by the anticancer drug dequalinium. *Mutat Res* 572:84–97. <https://doi.org/10.1016/j.mrfmmm.2004.12.010>.
 19. Hugo WB, Frier M. 1969. Mode of action of the antibacterial compound dequalinium acetate. *Appl Microbiol* 17:118–127. <https://doi.org/10.1128/am.17.1.118-127.1969>.
 20. Inácio AS, Domingues NS, Nunes A, Martins PT, Moreno MJ, Estronca LM, Fernandes R, Moreno AJM, Borrego MJ, Gomes JP, Vaz WLC, Vieira OV. 2016. Quaternary ammonium surfactant structure determines selective toxicity towards bacteria: mechanisms of action and clinical implications in antibacterial prophylaxis. *J Antimicrob Chemother* 71:641–654. <https://doi.org/10.1093/jac/dkv405>.
 21. Fraimow HS, Greenman JB, Leviton IM, Dougherty TJ, Miller MH. 1991. Tobramycin uptake in *Escherichia coli* is driven by either electrical potential or ATP. *J Bacteriol* 173:2800–2808. <https://doi.org/10.1128/jb.173.9.2800-2808.1991>.
 22. Radlinski L, Rowe SE, Kartchner LB, Maile R, Cairns BA, Vitko NP, Gode CJ, Lachiewicz AM, Wolfgang MC, Conlon BP. 2017. *Pseudomonas aeruginosa* exoproducts determine antibiotic efficacy against *Staphylococcus aureus*. *PLoS Biol* 15:e2003981. <https://doi.org/10.1371/journal.pbio.2003981>.
 23. Meylan S, Porter CBM, Yang JH, Belenky P, Gutierrez A, Lobritz MA, Park J, Kim SH, Moskowitz SM, Collins JJ. 2017. Carbon sources tune antibiotic susceptibility in *Pseudomonas aeruginosa* via tricarboxylic acid cycle control. *Cell Chem Biol* 24:195–206. <https://doi.org/10.1016/j.chembiol.2016.12.015>.
 24. Figueiredo-Godoi LMA, Garcia MT, Pinto JG, Ferreira-Strixino J, Faustino EG, Pedrosa LLC, Junqueira JC. 2022. Antimicrobial photodynamic therapy mediated by fotenticine and methylene blue on planktonic growth, biofilms, and burn infections of *Acinetobacter baumannii*. *Antibiotics* 11: 619. <https://doi.org/10.3390/antibiotics11050619>.
 25. Santos AL, Liu D, Reed AK, Wyderka AM, van Venrooy A, Li JT, Li VD, Misiura M, Samoylova O, Beckham JL, Ayala-Orozco C, Kolomeisky AB, Alemany LB, Oliver A, Tegos GP, Tour JM. 2022. Light-activated molecular machines are fast-acting broad-spectrum antibacterials that target the membrane. *Sci Adv* 8:eabm2055. <https://doi.org/10.1126/sciadv.abm2055>.
 26. Javanmardi F, Emami A, Pirbonyeh N, Rajaei M, Hatam G, Keshavarzi A. 2019. Study of multidrug resistance in prevalent Gram-negative bacteria in burn patients in Iran: a systematic review and meta-analysis. *J Glob Antimicrob Resist* 19:64–72. <https://doi.org/10.1016/j.jgar.2019.04.017>.
 27. Guo L, Xu H, Yue Z. 2022. Antibiotic resistance pattern of *Pseudomonas aeruginosa* wound isolates among Chinese burn patients: a systematic review and meta analysis. *Asian Pac J Trop Med* 15:17–25. <https://doi.org/10.4103/1995-7645.335703>.
 28. Wiegand I, Hilpert K, Hancock RE. 2008. Agar and broth dilution methods to determine the minimal inhibitory concentration (MIC) of antimicrobial substances. *Nat Protoc* 3:163–175. <https://doi.org/10.1038/nprot.2007.521>.
 29. Fratini F, Mancini S, Turchi B, Friscia E, Pistelli L, Giusti G, Cerri D. 2017. A novel interpretation of the Fractional Inhibitory Concentration Index: the case *Origanum vulgare* L. and *Leptospermum scoparium* J. R. et G. Forst essential oils against *Staphylococcus aureus* strains. *Microbiol Res* 195: 11–17. <https://doi.org/10.1016/j.micres.2016.11.005>.
 30. Angelova M, Dimitrov DS. 1986. Liposome electroformation. *Faraday Discuss Chem Soc* 81:303–311. <https://doi.org/10.1039/dc9868100303>.
 31. Angelova M, Dimitrov DS. 1988. A mechanism of liposome electroformation, p 59–67. In Degiorgio V (ed), *Trends in colloid and interface science II*. Springer, Berlin, Germany.
 32. Angelova M. 2000. Giant vesicles, p 27–36. In Luisi PL, Walde P (ed), *Perspectives in supramolecular chemistry*. Wiley-Interscience, Chichester, UK.
 33. Lindsey H, Petersen NO, Chan SI. 1979. Physicochemical characterization of 1,2-diphytanoyl-sn-glycero-3-phosphocholine in model membrane systems. *Biochim Biophys Acta* 555:147–167. [https://doi.org/10.1016/0005-2736\(79\)90079-8](https://doi.org/10.1016/0005-2736(79)90079-8).
 34. Redwood WR, Pfeiffer FR, Weisbach JA, Thompson TE. 1971. Physical properties of bilayer membranes formed from a synthetic saturated phospholipid in n-decane. *Biochim Biophys Acta* 233:1–6. [https://doi.org/10.1016/0005-2736\(71\)90351-8](https://doi.org/10.1016/0005-2736(71)90351-8).
 35. Belanger CR, Hancock REW. 2021. Testing physiologically relevant conditions in minimal inhibitory concentration assays. *Nat Protoc* 16:3761–3774. <https://doi.org/10.1038/s41596-021-00572-8>.
 36. Regoes RR, Wiuff C, Zappala RM, Garner KN, Baquero F, Levin BR. 2004. Pharmacodynamic functions: a multiparameter approach to the design of antibiotic treatment regimens. *Antimicrob Agents Chemother* 48:3670–3676. <https://doi.org/10.1128/AAC.48.10.3670-3676.2004>.
 37. Maslova E, Shi Y, Sjöberg F, Azevedo HS, Wareham DW, McCarthy RR. 2020. An invertebrate burn wound model that recapitulates the hallmarks of burn trauma and infection seen in mammalian models. *Front Microbiol* 11:998. <https://doi.org/10.3389/fmicb.2020.00998>.